



# 1 Vertical distribution of aerosols over the Maritime 2 Continent during El Nino 3

4 Jason Blake Cohen<sup>1</sup>, Daniel Hui Loong Ng<sup>2</sup>, Alan Wei Lun Lim<sup>3</sup>, Xin Rong Chua<sup>4</sup>  
5

6 <sup>1</sup>School of Atmospheric Sciences, Sun Yat-Sen University, Guangzhou, China

7 <sup>2</sup>Tropical Marine Science Institute, National University of Singapore, Singapore

8 <sup>3</sup>The Chinese University of Hong Kong, Hong Kong, China

9 <sup>4</sup>Princeton University, Princeton, NJ, USA  
10

10

11 *Correspondence to:* Jason Blake Cohen (jasonbc@alum.mit.edu)

12

13 **Abstract.** The vertical distribution of aerosols over Southeast Asia, a critical factor of aerosol lifetime, and  
14 impact on radiative forcing and precipitation, is examined for the 2006 post El-Nino fire burning season.  
15 Additionally, through analysis of measurements and modeling, we have reconfirmed the hypothesis that fire  
16 radiative power is underestimated. Our results are significantly different from what others are using. The  
17 horizontally constrained Maritime Continent's fire plume median height, using the maximum variance of  
18 satellite observed Aerosol Optical Depth as the spatial and temporal constraint, is found to be  $2.17 \pm$   
19  $1.53\text{km}$  during the 2006 El Nino season. This is  $0.96\text{km}$  higher than random sampling and all other past  
20 studies, with 62% of particles in the free troposphere. The impact is that the aerosol lifetime will be  
21 significantly longer, and that the aerosols will disperse in a direction different from if they were in the  
22 boundary layer. Application of a simple plume rise model using measurements of fire properties  
23 underestimates the median plume height by  $0.34\text{km}$  and more in the bottom-half of the plume. The center  
24 of the plume can be reproduced when fire radiative power is increased by 20% (range from 0% to 100%).  
25 However, to reduce the biases found, improvements are required in terms of measurements of fire  
26 properties when cloud covered, representation of small scale convection, and inclusion of aerosol direct and  
27 semi-direct effects. The results provide the unique aerosol signature of fire under El-Nino conditions.



## 28 1. Introduction

29 Properly quantifying the vertical distribution of aerosols is essential to constrain their atmospheric  
30 distribution, and in turn, the atmospheric energy budget [Ming *et al.*, 2010; Kim *et al.*, 2008], and  
31 understand their impact on circulation, clouds and precipitation [Tao *et al.*, 2012; Wang 2013], and human  
32 health [Burnett *et al.*, 2014]. However, there are complicating factors including spatial and temporal  
33 heterogeneity in emissions [Cohen and Wang, 2014; Cohen, 2014; Giglio *et al.*, 2006; Petrenko *et al.*, 2012;  
34 Wooster *et al.*, 2012], and uncertainties and non-linearities associated with aerosol processing and removal  
35 from the atmosphere [Tao *et al.*, 2012; Cohen and Prinn, 2011; Cohen *et al.*, 2011]. Furthermore, a lack of  
36 sufficiently dense measurements leads to difficulty constraining the measured distribution of aerosols over  
37 scales from hundreds to thousands of kilometers or over time frames on the decadal to longer time scales  
38 [Cohen and Wang, 2014; Delene and Ogren, 2002; Dubovik *et al.*, 2000; Cohen *et al.*, 2016].

39 Models do a poor job of reproducing the vertical distribution of aerosols [Cheng *et al.*, 2012;  
40 Schuster *et al.*, 2005; Tsigaridis *et al.*, 2014] as well as the related value of total column loading [Colarco *et al.*,  
41 2004; Leung *et al.*, 2007]. Furthermore, vertical measurements are sparse, often not providing adequate  
42 statistics to make informed comparisons with real world conditions. This is no more apparent than over  
43 Southeast Asia, where studies [Tosca *et al.*, 2011; Martin *et al.*, 2012] have concluded that the aerosol  
44 height is narrowly confined in the planetary boundary layer, although measurements throughout the region  
45 demonstrate otherwise [Lin *et al.*, 2014]. Presently, there are no known modeling efforts that have been able  
46 to reproduce this significant loading.

47 Additionally, aerosol emissions databases in Southeast Asia are quantified using a bottom-up  
48 approach, where small samples and statistics of the activity, land-use, economics, population, and hotspots  
49 are aggregated [van der Werf, 2010; Lamarque, 2010; Bond *et al.*, 2004]. This generally leads to significant  
50 bias, since there are few measurements and rapidly changing land-surface features over Southeast Asia. A  
51 recent couple of papers, using measurements and models in tandem, has quantified a significant  
52 underestimation in aerosol emissions over Southeast Asia in terms of magnitude [Cohen and Wang, 2014],  
53 spatial, and temporal distribution [Cohen, 2014], including interannual and intraannual variation from fires.

54 Furthermore, the vertical distribution is uncertain due to incomplete understanding of in-situ  
55 production and removal mechanisms, which are dependent on washout, which is also poorly modeled [Tao  
56 *et al.*, 2012; Wang 2013], especially in the tropics during the dry season [Petersen and Rutledge, 2001;  
57 Ekman *et al.*, 2012], due to the random nature of convective precipitation. Heterogeneous aerosol  
58 processing may also change the hygroscopicity and hence vertical distribution of the aerosols [Kim *et al.*,  
59 2008; Cohen *et al.*, 2011]. These factors have been shown to combine such that small changes in the initial  
60 vertical distribution can lead to ultimate transport thousands of kilometers apart [Wang, 2013].

61 The Maritime Continent of Southeast Asia has faced widespread and ubiquitous fires the past few  
62 decades, due to expanding agriculture, urban development, economic growth, and changes in the base  
63 climatology that induce drought [Center, 2005; Dennis *et al.*, 2005; van der Werf *et al.*, 2008; Taylor,  
64 2010]. These fires contribute the major fraction of the atmospheric aerosol burden during the dry season



65 [Cohen, 2014]. However, these fires are unique: they are relatively low in radiative power and temperature,  
66 yet cover a massive net surface area, making their statistics and extent hard to characterize from remote  
67 sensing. Yet, their total emissions are very high and they dominate the aerosol optical depth (AOD) and  
68 PM<sub>2.5</sub> levels over thousands of kilometers [Field *et al.*, 2009; Nakajima *et al.*, 1999]. Due to their  
69 widespread nature, fires in this region are geospatially coherent in their timing and geography, although  
70 individually they burn for different lengths of time, as a function of localized precipitation and soil  
71 moisture, and global circulation patterns such as El-Nino [Cohen, 2014; Wooster *et al.*, 2012; Hansen,  
72 2008].

73 This work describes a new approach to comprehensively sample the vertical distribution of smoke  
74 aerosols, by first using decadal scale measurements of AOD from the MISR satellite [Cohen, 2014], and  
75 then separating the smoke impacted regions by the magnitude of the measured variability. During the 2006  
76 El-Nino enhanced burning, one of the 2 largest such events over the past 15-year measurement record, this  
77 approach yields a much higher vertical aerosol height than the traditional random sampling approach. A  
78 simple plume-rise model [Achtemeier *et al.*, 2011; Briggs, 1965] using reanalysis meteorology [Kalnay *et al.*,  
79 1996] and measured fire properties was found to underestimate the measured heights. However, the  
80 model could be improved to match the median heights by increasing the measured fire radiative power  
81 [Sessions *et al.*, 2011; Sofiev *et al.*, 2012], implying that the measured fires may be underestimated in terms  
82 of their strength, or that there are missing fires. However, the top and bottom heights of the measured  
83 plume still cannot be reproduced. The data shows that an improved representation of both localized  
84 convective transport and the aerosol direct and semi-direct effects [Ekman *et al.*, 2007; Wang, 2007] are  
85 required to make further improvements. It is hoped that these results will provide insight to those working  
86 on understanding the strong 2015-2016 El-Nino conditions.

## 87 2. Methods

### 88 2.1 Geography

89 This work is focused on the Maritime Continent, a sub region of Southeast Asia (8°S to 8°N, 95°E  
90 to 125°E) (**Figure 1**) that experiences wide-spread and highly emitting fires on a yearly basis during the  
91 local dry season (August to October/November). The combined magnitude of the fires produces a single  
92 massive smoke plume, that covers much of the region, extending thousands of kilometers [Cohen, 2014].  
93 These wide spread fires are due to anthropogenic clearing of rainforest and agriculture [Cohen *et al.*, 2016;  
94 Dennis *et al.*, 2005; van der Werf *et al.*, 2008; Taylor, 2010; Miettinen *et al.*, 2013; Langmann *et al.*, 2009].  
95 Over this region, during the dry season, the removal of aerosols is quite slow, leading to the overall  
96 properties of the plume being relatively consistent over space and time [Cohen, 2014]. Therefore, the  
97 overall properties of the smoke plume, when correctly bounded in space and time, can be robustly  
98 statistically related to the overall properties of individual fires, and daily measurements of AOD from the  
99 MISR satellite (**Figure 1**) [Cohen, 2014].

100 In 2006, the El-Nino conditions led to an enhanced drought, with subsequent fires lasting from  
101 September through November. To ensure that the data analyzed is definitely from this event, only data from



102 October is used. The region in (**Figure 1**) with the EOF (Bjornsson and Venegas, 1997; Cohen et al., 2016)  
103 of the measured MISR AOD larger than 2.2 is the net of the source regions (over land) and downwind  
104 regions (over both land and sea), thereby providing a holistic representation of the impact of fires on the  
105 large-scale structure, and allows for a comprehensive sampling of the vertical distribution of the smoke,  
106 including observed fires, fires obscured by clouds (very common in this region), and aged aerosols directly  
107 downwind from their initial sources.

## 108 2.2 Measurements

109 CALIPSO is an active lidar that quantifies both the vertically resolved atmospheric backscatter  
110 strength (a reasonable approximation of the vertical profile of aerosols), and an indication of particle size  
111 (large or small) [Winker et al., 2003]. Specifically, we use the backscatter at 532nm and the vertical feature  
112 mask (vertical resolution 30m, horizontal resolution 1/3km) [Hostetler et al., 2006]. Since the width of each  
113 pass is narrow, they are not spatially representative in general. However, given the relative consistency of  
114 the plume as a whole, samples constrained within the plume's spatial extent, taken on the same day, are  
115 statistically representative of the smoke plume as a whole [Cohen, 2014].

116 The extinction-weighted top (10% vertically integrated height), middle-upper (30% vertically  
117 integrated height), median (50% vertically integrated height), middle-lower (70% vertically integrated  
118 height), and bottom (90% vertically integrated height) are computed for each individual measurement, with  
119 the values retained if the aerosol is not in the stratosphere (assumed to be 15km). The data is then  
120 aggregated first by day, and secondly by geography, either into the fire-impacted region, or non fire-  
121 impacted region, based on (**Figure 1**) [Cohen, 2014]. The aggregated set of measurements is used to  
122 compute probability densities and statistics, demonstrating the vast difference over the fire-impacted and  
123 non-fire impacted regions (**Figures 2a,2b**), with the vertical heights both significantly higher and less  
124 variable ( $p < 0.01$ ) over the fire region than the non-fire region.

125 Measurements of aerosol optical depth (AOD) [Kaufman et al., 2003], fire radiative power (FRP)  
126 and fire temperature ( $T_F$ ) [Freeborn et al., 2014; Ichoku et al., 2008] are obtained from the MODIS  
127 instrument aboard both the TERRA and AQUA satellites. Version 5, level 2, swath-by-swath measurements,  
128 at daily resolution are used for AOD (best solution 0.55 micron), with a spatial resolution of 10kmx10km,  
129 and FRP/ $T_F$ , with a spatial resolution of 1kmx1km. Given the prevalence of clouds in this region, the cloud-  
130 cleared products are used, leading to a possible low bias in the FRP/ $T_F$  measurements, as well as some fires  
131 not measured at all [Cohen et al., 2016; Freeborn et al., 2014; Ichoku et al., 2008; Kahn et al., 2008; Kahn  
132 et al., 2007]. On the other hand, while some grids are contaminated, the sheer spatial distance of the plume  
133 and the fact that the overwhelming majority of atmospheric aerosols during this time of the year are due to  
134 fires, means that there is no significant bias in the overall statistics of the measured AOD [Cohen, 2014], as  
135 observed by looking at the spatially averaged MODIS AOD and statistics over the fire-constrained and non  
136 fire-constrained regions (**Figure 3**). The AOD is significantly higher ( $p < 0.01$ ) over the fire-constrained  
137 region, making the findings consistent with the approach employing the 12 years worth of MISR  
138 measurements.



### 139 2.3 Plume Rise Model

140 A simple model is employed to simulate the height to which a parcel of air initially at the surface  
141 over the fire will rise, based on buoyancy, vertical, and horizontal advection (**Supplement**). The  
142 formulation requires information about the temperature and radiative power of the fire as well as local  
143 meteorology [*Achtemeier et al.*, 2011; *Briggs*, 1965], and yields an idealized height to which aerosols  
144 emitted will rise. The buoyant plume rise is a thermodynamic approximation in nature and thus not as  
145 physically realistic as a large eddy approach, which solves the atmospheric fluid dynamical equations by  
146 parameterizing turbulence at the scale of tens of meters. However, it is less computationally expensive and  
147 more generalizable in the context of approximating the thousands of fires spread geographically over  
148 hundreds of thousands of square kilometers. On the other hand, it is more physically realistic than empirical  
149 relationships from multi-angle measurements [*Sofiev et al.*, 2012], which have also been attempted, but  
150 show poor performance in Southeast Asia.

151 These relationships are efficiently solved using measurements of meteorological and fire  
152 properties, allowing them to be used as rapid parameterizations within regional or global models. However,  
153 there are errors associated with reconciling the different temporal and spatial scales of reanalysis  
154 meteorology, especially convection and associated transport. Secondly, cloud-cover in this region leads to  
155 both missing fires and low-bias in measurements of fire properties [*Sofiev et al.*, 2012; *Kaufman et al.*,  
156 2003]. Third, the cloud-cover also leads to a heavier contribution of model results in the reanalysis  
157 meteorology. Finally, the effects of the optically thick aerosol plume's feedback on the radiative profile is  
158 likely significant, but not taken into consideration [*Ekman et al.*, 2007; *Wang*, 2007].

## 159 3. Results and Discussion

### 160 3.1 Measured Aerosol Vertical Distribution

161 The fire-constrained monthly aggregated daily statistics of the measured vertical aerosol height  
162 from CALIPSO [*Winker et al.*, 2003] is given in (**Figure 2a**), with the monthly aggregated statistics over  
163 the fire-constrained region of the bottom, middle-lower, median, middle-upper, and top heights  
164 respectively:  $1.68 \pm 1.59\text{km}$ ,  $1.92 \pm 1.55\text{km}$ ,  $2.17 \pm 1.53\text{km}$ ,  $2.50 \pm 1.54\text{km}$ , and  $2.98 \pm 1.55\text{km}$  (**Table**  
165 **1**). On the other hand, the non fire-constrained region's monthly aggregated statistics of the measured  
166 vertical aerosol height is quite different (**Figure 2b**), with the respective bottom, middle-lower, median,  
167 middle-upper, and top heights:  $0.65 \pm 0.98\text{km}$ ,  $0.93 \pm 0.98\text{km}$ ,  $1.21 \pm 1.00\text{km}$ ,  $1.53 \pm 1.02\text{km}$ , and  
168  $1.98 \pm 1.08\text{km}$  (**Table 1**). The average aerosol height over the fire-constrained region is both much higher  
169 and more variable at every vertical level as compared to the non fire-constrained domain, with 62% of the  
170 aerosol loading in the free troposphere over the fire-constrained domain, while only 17% is located in the  
171 free troposphere over the non fire-constrained domain. However, the variability is roughly constant at all  
172 levels over the fire-constrained region, while the variability increases with vertical level, over the non fire-  
173 constrained region.

174 All three findings, higher average aerosol height, larger variance of height, and a consistent  
175 variance of height at all levels, are consistent with areas where most of the aerosol loading is due to surface



176 fires. Firstly, the buoyancy from fires increases the expected height, with differences in buoyancy from  
177 different strength fires producing random variability in the measured heights. So long as the distribution of  
178 fire strength and meteorology do not differ too much from day-to-day, the variance in aerosol heights  
179 should also not vary much. On the other hand, over non fire-constrained regions, the major contribution to  
180 the vertical aerosol variability is convection, which is expected to increase in variability the higher one  
181 moves upwards from the surface.

182 Furthermore, the relatively constant variability across the heights in the fire-constrained region is  
183 consistent with a proposed radiative-stabilization effect. The extremely high measured AOD values found  
184 by MODIS [Kaufman *et al.*, 2003] over the fire-constrained domain (from 0.5 to 2.0, with most days over  
185 1.0), leads to significant surface cooling (**Figure 3**). Additionally, BC emitted from the fire, absorbs  
186 incoming solar radiation near the upper portion of the plume, providing a significant warming. This  
187 combination leads to additional stabilization of the atmosphere, and therefore the vertical aerosol  
188 distribution.

189 These results are thus consistent with the observed reduction in in-situ vertical processing over the  
190 regions downwind from the fire sources, but still within the fire-constrained plume region, where buoyancy  
191 from the fires and the self-stabilization effect seem to contribute more than random deep convection.  
192 However, over the non fire-constrained region, given the low AOD and lack of fires, both of these effects  
193 are not observed, and convection dominates, which is consistent with the less uniform vertical distribution.  
194 Given these clear and observed differences, only results from the fire-constrained region will be considered  
195 further.

196 A significant amount of aerosol mass exists in the free troposphere over this region. By assuming  
197 that the measured boundary layer height of 1000m as observed in Singapore [Chew *et al.*, 2013] is applied  
198 to the domain, then 62%, 73%, 83%, 93%, and 98% of the total monthly respective measurements of the  
199 bottom, lower-middle, median, upper-middle and top extinction heights are located in the free troposphere.  
200 This is much higher than previous studies, which indicated most of the smoke remained within the  
201 boundary layer [Tosca *et al.*, 2011].

202 Analysis of the daily measured heights demonstrates 3 statistically unique days: October 11<sup>th</sup>, 15<sup>th</sup>  
203 and 22<sup>nd</sup> (**Table 2**). On the 11<sup>th</sup>, the top and upper-middle measurements fall within the top 15%, while the  
204 median measurements fall within the top 20% of the month's measurements, implying that the result is  
205 consistent with a deep, single layer, extending throughout the lower and middle free-troposphere. The 15<sup>th</sup>  
206 and 22<sup>nd</sup>, while not being as high in the middle-troposphere, also have little to no aerosol in the planetary  
207 boundary layer due to being significantly more confined in the vertical, implying a narrow layer in the  
208 middle free-troposphere. These results are consistent with the measured aerosol layer being mostly in the  
209 free troposphere, a result that is not consistent with the measured FRP or meteorology, leading to two  
210 important implications. Firstly, the aerosol lifetime on these days will be considerably longer than models  
211 typically reproduce and the radiative forcing will be considerably more warming. Secondly, that typical  
212 modeling approach that fresh aerosols are mixed from the surface to the given top of the plume height is



213 likely not true here, which has implications for the ability of most models to be able to correctly capture the  
214 aerosol loading.

215 On the remaining days, the measured heights are consistent on a daily average basis with relatively  
216 uniform emissions, meteorology, and vertical buoyant rise. Although present, intense but heterogeneous  
217 forcing impacting the vertical distribution, such as localized convection and aerosol cloud interactions are  
218 generally not observed to bias the overall plume's properties. Only on October 11<sup>th</sup>, 15<sup>th</sup>, and 22<sup>nd</sup>, are there  
219 significantly higher heights or a narrower vertical structure, combined with no readily available explanation  
220 to be found in the fire, AOD, or meteorological properties on these days, indicating a likely significant  
221 change in the convection on those days, or some other phenomena not considered or captured by the  
222 reanalysis meteorology. The robustness of this approach assures the validity over the region and time period  
223 considered herein.

### 224 3.2 Measured Fire and Meteorological Properties

225 The daily aggregated measurements of fire radiative power (FRP) [Freeborn *et al.*, 2014; Ichoku *et al.*, 2008]  
226 indicate there are 109395 actively burning 1kmx1km pixels in October 2006. However, filtering  
227 for high confidence [Level 9] active fires, reduces this number to 6941 1kmx1km pixels. The respective  
228 measurements have 10%, median, and 90% values of FRP of [115,300,975] W/m<sup>2</sup> for all fires and  
229 [185,540,1495] W/m<sup>2</sup> for high confidence fires (**Table 3**). Overall, these values are significantly lower than  
230 FRP measured over other intensely burning regions [Giglio *et al.*, 2006]. However, the results are consistent  
231 with the fact that fires in the Maritime Continent occur under relatively wet surface conditions, due to high  
232 levels of mineral-soil moisture, extensive peat, and intermittent localized precipitation [Couwenberg *et al.*,  
233 2010].

234 There is only one day, October 2<sup>nd</sup>, with a significantly high FRP (daily mean more than monthly  
235 90% value), for high confidence fires. Similarly, there are two days, October 28<sup>th</sup> and 30<sup>th</sup>, with an  
236 abnormally low FRP (daily mean less than monthly 15% value), for high confidence fires. None of these  
237 days have a significantly abnormal fire vertical height distribution. However, October 28<sup>th</sup> and 30<sup>th</sup> both  
238 show a significant increase in AOD over the fire constrained region, with the AOD more than 2 standard  
239 deviations greater than the mean over the non fire constrained region, as compared to the period of time  
240 from the 25th through the 27th. One consistent rationale is that there was large-scale precipitation increasing  
241 aerosol removal and subsequently wetting the surface. This in turn led to lower temperature and FRP and  
242 correspondingly higher aerosol emissions factor on these days. Overall, there is no apparent impact of day-  
243 to-day variability of measured FRP driving observed variation in measured aerosol heights, and hence only  
244 high confidence fire data is subsequently used.

245 MERRA [Rienecker *et al.*, 2011] reanalysis meteorology is used for the horizontal and vertical  
246 wind, and vertical temperature profile at each location where a fire is measured (**Table 3**). MERRA was  
247 chosen because it is based on NASA satellite measurements, and thus should be more consistent with the  
248 measurements used here. With the exceptions of October 5<sup>th</sup> and 20<sup>th</sup>, the horizontal wind is relatively calm  
249  $6.0 \pm 1.3$  m/s. Also, throughout the entire month, the vertical temperature gradient is relatively stable





250  $-5.45 \pm 0.16\text{K/km}$ , with only 7 individual fires occurring under unstable atmospheric conditions.  
251 Therefore, dynamical instability is not expected to contribute significantly to the vertical distribution [Stone  
252 and Carlson, 1979]. Also, the role played by the large-scale vertical wind is small  $2.1 \pm 1.6\text{mm/s}$ . Given  
253 the atmospheric stability and fire-controlled buoyancy conditions, the plume rise model approach should  
254 offer a reasonable approximation of the aerosol vertical distribution.

255 The approach used here relies upon the atmosphere being either stable or only minority non-stable.  
256 However, in general in this part of the world, there are two reasons that would contribute to most fires  
257 occurring under such conditions: firstly, that major instability would frequently lead to rain, fire  
258 suppression, and aerosol wash-out; and secondly that the induced surface cooling and atmospheric heating  
259 by the extensive aerosol layer itself would tend to increase the atmospheric stability. Such points are made  
260 clear in terms of the major unaccounted for processes in the MERRA data at this resolution, being:  
261 localized convection (due to the resolution), and the aerosol cooling and in-situ heating effects (not  
262 incorporated into MERRA's underlying model). In theory the direct and semi-direct effect may be able to  
263 be parameterized, but this would require a higher order model. Hence, since these conditions and effects are  
264 not considered by the plume rise model, they therefore cannot be explanations for discrepancies in the  
265 modeled vertical distribution.

### 266 3.3 Modeled Aerosol Vertical Distribution

267 Applying the plume rise model, the aggregated daily statistics of the vertical aerosol height at the  
268 bottom, lower-middle, median, upper-middle, and top are 0.60km, 1.14km, 1.85km, 2.87km, and 4.99km  
269 respectively (**Figure 4, Table 4**). The mean daily median, lower-middle, and bottom modeled heights are  
270 lower than the respective mean measured heights by 0.48km, 0.78km, and 1.07km respectively, with a wide  
271 underestimate day-to-day ranging from 1.91km to 1.11km. The upper-middle modeled height is about equal  
272 to measurements, with a mean difference of 0.03km, and wide day-to-day variations, from an overestimate  
273 of 1.97km to an underestimate of 1.36km. Finally, the top modeled heights are significantly higher than  
274 measurements, with an average overestimate of 1.02km, and a day-to-day range from an overestimate of  
275 3.96km to an underestimate of 0.44km.

276 The model underestimates the height of the median through bottom of the plume, while  
277 simultaneously overestimating the top. First, this means that the model is not accounting for enough energy  
278 to obtain the average rise of the plume. At the same time, the modeled vertical spread is too large, implying  
279 other factors limit the height gain near the top of the plume while simultaneously enhance the height near  
280 the bottom. The results are consistent with one or both of the two hypothesized effects; first, that a low bias  
281 exists in the measured values of FRP [Kahn *et al.*, 2007; Kahn *et al.*, 2008, leading to insufficient  
282 buoyancy; and second, that in-situ stabilization occurs due to aerosol radiative cooling in the lower parts of  
283 the plume and aerosol radiative heating within the upper parts of the plume. This combination of factors is  
284 also consistent with the observed underestimate in measured FRP to match the median height, as well as the  
285 hypothesized complete non-detection of small fires [Kaufman *et al.*, 2003]. There are also uncertainties in  
286 the MERRA reanalysis products, but given the large sample size and the narrowness of the MERRA





287 distribution, the impact of these uncertainties is considerably smaller than changes in the FRP on the order  
288 of 10%.

289 A sensitivity analysis is used to quantify the effects of a low bias in FRP, by applying a constant  
290 multiplicative factor to the measured FRP for each fire, from 1.0 to 2.0 in steps of 0.1 (although only the  
291 results in steps of 0.2 are given in **Table 4**). Although there are also uncertainties associated with measured  
292 vertical wind and temperature structure, this is not considered (**Table 3**), since there is no way to couple  
293 meteorological effects at sub-grid scale, or otherwise not included in the reanalysis meteorology. The  
294 results are obtained by minimizing the root-mean square (RMS) difference between the daily measured and  
295 modeled heights, for each FRP scaling factor, at each of the middle-upper, median, and middle-lower  
296 levels. The respective best-fit enhancement factors are **1.0** for middle-upper measurements (RMS=0.94km),  
297 **1.2** for median measurements (RMS=0.81km), and **2.0** for middle-lower measurements (RMS=0.74km)  
298 (**Table 4**). Although there is no single best-fit FRP scaling factor, the results produce a better fit to  
299 measured values from the middle-lower to the middle-upper than using the model without any FRP  
300 enhancement.

301 The results establish that current plume rise models can reproduce the median vertical plume  
302 height over Southeast Asia by increasing the FRP by 20%, a finding consistent with FRP generally  
303 underestimated over this region. By changing the FRP enhancement from 0% to 100%, the central height of  
304 the plume can be modeled, although the top and bottom heights of the plume cannot be reproduced.  
305 Additionally, the modeled plume is widely spread as compared to the narrowness of the measured plume.  
306 Unfortunately, rectifying these limitations will likely require the use of a more complex modeling approach  
307 and improvement of measured fire data.

## 308 4. Conclusions

309 This work comprehensively quantifies the significant present-day underestimation of the vertical  
310 distribution of aerosols over the Maritime Continent during an El-Nino influenced fire season, by  
311 introducing a new method to appropriately constrain the measurements over the geographical region of the  
312 aerosol plume. The measured heights over the constrained region are found to be higher than previously  
313 thought, with about 62% of aerosols found in the free troposphere, where they can be advected thousands  
314 of kilometers and have more impact on the atmospheric and climatic systems. Additionally, over the fire-  
315 constrained region, the vertical variability of the plume is found to be uniform throughout its height,  
316 implying that it is controlled mostly by local forcing, such as the buoyancy released by fires, localized  
317 convection, and aerosol/radiative feedbacks, such as the direct and semi-direct effects.

318 Application of a plume-rise model showed that there was an overall low bias against measured  
319 heights, which is consistent with the FRP being underestimated in this region of the world due to large-  
320 scale cloud cover. It was also determined that measured vertical heights are more narrowly confined than  
321 model simulations. Applying a robust sensitivity analysis found that the middle-lower through middle-  
322 upper extent of the plume can be reproduced if an appropriate (although changing) enhancement is applied  
323 to the FRP ranging from  $1.0 \cdot \text{FRP}$  to  $2.0 \cdot \text{FRP}$  (with  $1.2 \cdot \text{FRP}$  the best fit-value). Hence, the variable FRP



324 enhancement factor approach can allow for improved modeling of the height statistics for the middle-upper  
325 to middle-lower extent of the plume.

326 However, it is not possible to reproduce either the top or bottom of the measured heights, the  
327 knowledge of which is important to constrain the impacts of long-range transport and aerosol-climate  
328 interactions. Nor is it possible to reproduce the narrow spread of the measured heights. The results are  
329 consistent with the general understanding of current model shortcomings, which in addition to the  
330 underestimated FRP values, will also need to be addressed. Hence, the current community-wide  
331 dependence on FRP measurements for vertical aerosol modeling may lead to flaws in our being able to  
332 successfully model the distribution.

333 The results have been found to be robust over a region that behaves roughly uniformly over  
334 thousands of kilometers and includes regions both near and far from the source of the fires. Since there are  
335 only a few days that have relatively unique aerosol and meteorological properties over the period studied,  
336 the results support the most important aspect of improving the aerosol heights will be newer modelling  
337 approaches and improvements that will be able to resolve local-scale forcing, such as deep convection,  
338 aerosol/radiation interactions, and aerosol-cloud interactions. Secondly, the biased underestimation of FRP  
339 is also an important point to improve the aerosol height modeling, especially under conditions where  
340 cloudiness occurs or the measured AOD levels are very high. These errors are exacerbated over regions  
341 where large-scale precipitation is very low or where there is significant aerosol/cloud intermixing. In all  
342 cases, until these model and measurement improvements are made, there is expected to be a significant  
343 underestimation of the aerosol loadings and radiative forcing distribution regionally, and to some extent  
344 globally. It is hoped that in the interim, the community will adapt a variable enhancement of FRP in tandem  
345 with measurement-constrained boundaries of smoke plumes, as a way to more precisely reproduce the  
346 statistics of the vertical aerosol distribution.



347 **Acknowledgements:**

348 We would like to acknowledge the PIs of the NASA MODIS, MISR, and CALIPSO projects for providing  
349 the data. The work was supported financially by the Young Thousand Talents Program of the Chinese  
350 National Government, and Project 74110-41110002 of the Chinese Ministry of Science and Technology.



351 **References:**

- 352 Achtemeier, G., S. Goodrick, Y. Liu, F. Garcia-Menendez, Y. Hu, and M. Odman, (2011). Modeling smoke  
353 plume-rise and dispersion from Southern United States prescribed burns with daysmoke.  
354 *Atmosphere*, 2, 358-388.
- 355 Bjornsson, H. and Venegas, S, (1997). A Manual for EOF and SVD Analyses of Climate Data. Department  
356 of Atmospheric and Oceanic Sciences and Centre for Climate and Global Change Research, Tech.  
357 rep., McGill University, Technical Report, 1997.
- 358 Bond, T. C., D.G. Streets, K.F. Yarber, S.M. Nelson, J.H. Woo, and Z. Klimont. (2004). A technology-based  
359 global inventory of black and organic carbon emissions from combustion, *J. Geophys. Res.*, 109,  
360 D14203, doi:10.1029/2003JD003697.
- 361 Briggs, G. A. (1965). A plume rise model compared with observations. *Journal of the Air Pollution Control*  
362 *Association*, vol. 15, no. 9, pp. 433–438.
- 363 Burnett, R., A. Pope, M. Ezzati, C. Olives, S. Lim, S. Mehta, H. Shin, G. Singh, B. Hubbell, M. Brauer, R.  
364 Anderson, K. Smith, J. Balmes, N. Bruce, H. Kan, F. Laden, A. Pruss-Ustun, M. Turner, S. Gapstur,  
365 R. Diver, and A. Cohen. (2014) An Integrated Risk Function for Estimating the Global Burden of  
366 Disease Attributable to Ambient Fine Particulate Matter Exposure, *Environ Health Perspect*;  
367 doi:10.1289/ehp.1307049.
- 368 Chew, B. N., J.R. Campbell, S.V. Salinas, C.W. Chang, J.S. Reid, E.J. Welton, and S.C. Liew. (2013).  
369 Aerosol particle vertical distributions and optical properties over Singapore. *Atmospheric*  
370 *Environment*, 79, 599-613.
- 371 Chung, C. E., V. Ramanathan and D. Decremer. (2012) Observationally constrained estimates of  
372 carbonaceous aerosol radiative forcing, *Proc. Natl. Acad. Sci. U.S.A.*,  
373 doi:10.1073/pnas.1203707109.
- 374 Cohen, J. B. (2014) Quantifying the occurrence and magnitude of the Southeast Asian fire climatology.  
375 *Environmental Research Letters*, 9(11), 114018.
- 376 Cohen, J. B., Lecoq, E., and Hui Loong Ng, D.: Decadal-scale relationship between measurements of  
377 aerosols, land-use change, and fire over Southeast Asia, *Atmos. Chem. Phys.*, 17, 721-743,  
378 doi:10.5194/acp-17-721-2017, 2017.
- 379 Cohen, J. B. and Wang C (2014) Estimating Global Black Carbon Emissions Using a Top-Down Kalman  
380 Filter Approach. *J. Geophys. Res.*, doi:10.1002/2013JD019912.
- 381 Colarco, P., M. Schoeberl, B. Doddridge, L. Marufu, O. Torres, and E. Welton. (2004) Transport of smoke  
382 from Canadian forest fires to the surface near Washington, D.C.: Injection height, entrainment, and  
383 optical properties, *J. Geophys. Res.*, 109, D06203, doi:10.1029/2003jd00424.
- 384 Couwenberg, J., R. Dommain, and H. Joosten, H. (2010). Greenhouse gas fluxes from tropical peatlands in  
385 south-east Asia. *Global Change Biology*, 16: 1715–1732. doi:10.1111/j.1365-2486.2009.02016.
- 386 Delene, D. J. and J.A. Ogren (2002) Variability of aerosol optical properties at four North American  
387 surface monitoring sites, *J. Atmos. Sci.*, 59(6), 1135–1150.



- 388 Dennis, R. A., J. Mayer, G. Applegate, U. Chokkalingam, C.J.P. Colfer, I. Kurniawan, and T.P. Tomich.  
389 (2005). Fire, people and pixels: linking social science and remote sensing to understand underlying  
390 causes and impacts of fires in Indonesia. *Human Ecology*, 33(4), 465-504.
- 391 Dubovik, O., A. Smirnov, B.N. Holben, M.D. King, Y.J. Kaufman, T.F. Eck and I Slutsker. (2000)  
392 Accuracy assessments of aerosol optical properties retrieved from Aerosol Robotic Network  
393 (AERONET) Sun and sky radiance measurements. *J. Geophys. Res.*, 105(D8), 9791-9806.
- 394 Ekman, A., A. Engstrom and C. Wang. (2007). The effect of aerosol composition and concentration on the  
395 development and anvil properties of a continental deep convective cloud, *Q. J. Roy. Meteor. Soc.*,  
396 133B(627), 1439-1452.
- 397 Ekman, A. M. L., M. Hermann, P. Gross, J. Heintzenberg, D. Kim, and C. Wang. (2012). Sub-micrometer  
398 aerosol particles in the upper troposphere/lowermost stratosphere as measured by CARIBIC and  
399 modeled using the MIT-CAM3 global climate model, *J. Geophys. Res.*, 117, D11202,  
400 doi:10.1029/2011JD016777.
- 401 Field, R. D., G.R. van der Werf, S.P.P. Shen. (2009) Human amplification of drought-induced biomass  
402 burning in Indonesia since 1960. *Nature Geosci.*, 10.1038/ngeo443.
- 403 Freeborn, P. H., M.J. Wooster, D.P. Roy and M.A. Cochrane. (2014). Quantification of MODIS fire  
404 radiative power (FRP) measurement uncertainty for use in satellite-based active fire characterization  
405 and biomass burning estimation, *Geophys. Res. Lett.*, 41, 1988–1994, doi:10.1002/2013GL59086.
- 406 Giglio, L., I. Csiszar and C.O. Justice. (2006) Global distribution and seasonality of active fires as observed  
407 with the Terra and Aqua MODIS sensors. *J. Geophys. Res.*, doi:10.1029/2005JG000142.
- 408 Hansen, M. C. (2008). Humid tropical forest clearing from 2000 to 2005 quantified by using multitemporal  
409 and multiresolution remotely sensed data. *Proc. Natl. Acad. Sci. USA*, 105, 9439–9444.
- 410 Hostetler, C, Z. Liu, J. Reagan, M. Vaughan, D. Winker, M. Osborn, W. Hunt, K. Powell, and C. Trepte.  
411 (2006). CALIOP Algorithm Theoretical Basis Document–Part 1: Calibration and Level 1 Data  
412 Products. *Doc. PC-SCI* 201.
- 413 Ichoku, C., L. Giglio, M. Wooster and L. Remer. (2008). Global characterization of biomass-burning  
414 patterns using satellite measurements of fire radiative energy. *Remote Sensing of Environment* 112.6,  
415 2950-2962.
- 416 Kahn, R.A., Chen, Y., Nelson, D.L., Leung, F.Y., Li, Q.B., Diner, D.J., and Logan, J.A. (2008). Wildfire  
417 smoke injection heights: Two perspectives from space. *Geophys. Res. Lett.*, 35, L04809,  
418 doi:10.1029/2007GL032165.
- 419 Kahn, R.A., Li, W.H., Moroney, C., Diner, D.J., Martonchik, J.V., and Fishbein, E. (2007). Aerosol source  
420 plume physical characteristics from space-based multiangle imaging. *J. Geophys. Res.*, 112,  
421 D11205, doi:10.1029/2006JD007647, 2007
- 422 Kalnay et al. (1996). The NCEP/NCAR 40-year reanalysis project, *Bull. Amer. Meteor. Soc.*, 77, 437-470.



- 423 Kaufman, Y. J., C. Ichoku, L. Giglio, S. Korontzi, D.A. Chu, W.M. Hao, and C.O. Justice. (2003). Fire and  
424 smoke observed from the Earth Observing System MODIS instrument--products, validation, and  
425 operational use. *International Journal of Remote Sensing*, 24(8), 1765-1781.
- 426 Kim, D., C. Wang, A.M.L. Ekman, M. C. Barth, and P. Rasch. (2008) Distribution and direct radiative  
427 forcing of carbonaceous and sulfate aerosols in an interactive size-resolving aerosol-climate model,  
428 *J. Geophys. Res.*, 113, D16309, doi:10.1029/2007JD009756.
- 429 Lamarque, J. F. (2010). Historical (1850–2000) gridded anthropogenic and biomass burning emissions of  
430 reactive gases and aerosols: methodology and application. *Atmos. Chem. Phys.*, doi:10.5194/acp-10-  
431 7017-2010.
- 432 Langmann, B., B. Duncan, C. Textor, J. Trentmann, and G.R. van der Werf. (2009). Vegetation fire  
433 emissions and their impact on air pollution and climate. *Atmospheric Environment*, 43(1), 107-116.
- 434 Leung, F.Y.T., J.A. Logan, R. Park, E. Hyer, E. Kasischke, D. Streets, and L. Yurganov. (2007) Impacts of  
435 enhanced biomass burning in the boreal forests in 1998 on tropospheric chemistry and the sensitivity  
436 of model results to the injection height to emissions. *J. Geophys. Res.*, 112, D10313,  
437 doi:10.1029/2006JD008132.
- 438 Lin, N. H., A.M. Sayer, S.H. Wang, A.M. Loftus, T.C. Hsiao, G.R. Sheu, and S. Chantara. (2014).  
439 Interactions between biomass-burning aerosols and clouds over Southeast Asia: Current status,  
440 challenges, and perspectives. *Environmental Pollution*, 195, 292-307.
- 441 Martin, V.M., R.A. Kahn, J.A. Logan, R. Paugam, M. Wooster, and C. Ichoku. (2012). Space-based  
442 observational constraints for 1-D fire smoke plume-rise models. *Journal of Geophysical Research:*  
443 *Atmospheres (1984–2012)*, 117(D22).
- 444 Miettinen, J., E. Hyer, A.S. Chia, L.K. Kwoh, and S.C. Liew, S. C. (2013). Detection of vegetation fires  
445 and burnt areas by remote sensing in insular Southeast Asian conditions: current status of knowledge  
446 and future challenges. *International journal of remote sensing*, 34(12), 4344-4366.
- 447 Ming, Y., V. Ramaswamy and G. Persad. (2010) Two opposing effects of absorbing aerosols on global-  
448 mean precipitation. *Geophysical Research Letters* 37.13.
- 449 Nakajima, T., A. Higurashi, N. Takeuchi and J.R. Herman (1999). Satellite and ground-based study of  
450 optical properties of 1997 Indonesian Forest Fire aerosols. *Geophys. Res. Lett.*,  
451 10.1029/1999GL900208.
- 452 Petersen, W. and S. Rutledge. (2001). Regional Variability in Tropical Convection: Observations from  
453 TRMM. *J. Climate*, 14, 3566–3586.
- 454 Petrenko, M., R.A. Kahn, M. Chin, A.J. Soja, T. Kucsera, and Harshvardhan. (2012) The use of satellite-  
455 measured aerosol optical depth to constrain biomass burning emissions source strength in the global  
456 model GOCART, *J. Geophys. Res.*, doi:10.1029/2012JD01787.
- 457 Rienecker, M.M., M.J. Suarez, R. Gelaro, R. Todling, J. Bacmeister, E. Liu, M.G. Bosilovich, S.D.  
458 Schubert, L. Takacs, G.-K. Kim, S. Bloom, J. Chen, D. Collins, A. Conaty, and A. da Silva (2011).  
459 MERRA: NASA's Modern-Era Retrospective Analysis for Research and Applications. *J. Climate*,



- 460 24, 3624-3648, doi:10.1175/JCLI-D-11-00015.1
- 461 Schuster, G. L., O. Dubovik, B. Holben and E. Clothiaux. (2005) Inferring black carbon content and  
 462 specific absorption from Aerosol Robotic Network (AERONET) aerosol retrievals, *J. Geophys.*  
 463 *Res.*, 110, D10S17, doi:10.1029/2004JD004548.
- 464 Sessions, W. R., H.E. Fuelberg, R.A. Kahn, and D.M. Winker. (2011). An investigation of methods for  
 465 injecting emissions from boreal wildfires using WRF-Chem during ARCTAS. *Atmospheric*  
 466 *Chemistry and Physics*, 11(12), 5719-5744.
- 467 Sofiev, M., T. Ermakova, and R. Vankevich. (2012). Evaluation of the smoke-injection height from  
 468 wildland fires using remote-sensing data. *Atmos. Chem. Phys.*, vol. 12, no. 4, pp. 1995–2006.
- 469 Stone, P. and J. Carlson. (1979). Atmospheric Lapse Rate Regimes and Their Parameterization. *J. Atmos.*  
 470 *Sci.*, 36, 415–423.
- 471 Tao, W.K., J.P. Chen, Z.Q. Li, C. Wang, and C.D. Zhang. (2012) The Impact of Aerosol on convective  
 472 cloud and precipitation. *Rev. Geophys.*, 50, RG2001, doi:10.1029/2011RG000369.
- 473 Taylor, D. (2010). Biomass burning, humans and climate change in Southeast Asia. *Biodiversity and*  
 474 *conservation*, 19(4), 1025-1042.
- 475 Tosca, M. G., J.T. Randerson, C.S. Zender, D.L. Nelson, D.J. Diner, and J.A. Logan (2011), Dynamics of  
 476 fire plumes and smoke clouds associated with peat and deforestation fires in Indonesia, *J. Geophys.*  
 477 *Res.*, 116, D08207, doi:10.1029/2010JD015148.
- 478 Tsigaridis, K., N. Daskalakis, M. Kanakidou, P.J. Adams, P. Artaxo, R. Bahadur, Y. Balkanski, S.E.  
 479 Bauer, N. Bellouin, A. Benedetti, T. Bergman, T.K. Berntsen, J.P. Beukes, H. Bian, K.S.  
 480 Carslaw, K. S., M. Chin, G. Curci, T. Diehl, R.C. Easter, S.J. Ghan, S.L., Gong, A. Hodzic, C.R.  
 481 Hoyle, T. Iversen, S. Jathar, J.L. Jimenez, J.W. Kaiser, A. Kirkevåg, D. Koch, H. Kokkola, Y.H.  
 482 Lee, G. Lin, X. Liu, C. Luo, X. Ma, G.W. Mann, N. Mihalopoulos, J.J. Morcrette, J.F. Müller, G.  
 483 Myhre, S. Myriokefalitakis, N.L. Ng, D. O'Donnell, J.E. Penner, L. Pozzoli, K.J. Pringle, L.M.  
 484 Russell, M. Schulz, J. Sciare, O. Seland, D.T. Shindell, S. Sillman, R.B. Skeie, D. Spracklen, T.  
 485 Stavrakou, S.D. Steenrod, T. Takemura, P. Tiitta, S. Tilmes, H. Tost, T. van Noije, P.G. van Zyl, K.  
 486 von Salzen, F. Yu, Z. Wang, Z. Wang, R.A. Zaveri, H. Zhang, K. Zhang, Q. Zhang, and X.  
 487 Zhang, X. (2014) The AeroCom evaluation and intercomparison of organic aerosol in global  
 488 models, *Atmos. Chem. Phys.*, 14, 10845-10895, doi:10.5194/acp-14-10845-2014.
- 489 van der Werf, G. R. (2010). Global fire emissions and the contribution of deforestation, savanna, forest,  
 490 agricultural, and peat fires (1997–2009). *Atmos. Chem. Phys.*, 10.5194/acp-10-11707-2010.
- 491 van der Werf, G. R., J. Dempewolf, S.N. Trigg, J.T. Randerson, P.S. Kasibhatla, L. Giglio, and R.S DeFries.  
 492 (2008). Climate regulation of fire emissions and deforestation in equatorial Asia. *Proceedings of the*  
 493 *National Academy of Sciences*, 105(51), 20350-20355.
- 494 Wang, C. (2013) Impact of anthropogenic absorbing aerosols on clouds and precipitation: A review of  
 495 recent progresses, *Atmos. Res.*, 122, 237-249.
- 496 Wang, C. (2007). Impact of direct radiative forcing of black carbon aerosols on tropical convective





- 497 precipitation, *Geophys. Res. Lett.*, 34, L05709, doi:10.1029/2006GL028416.
- 498 Winker, D. M., J. Pelon, and M.P. McCormick (2003), The CALIPSO mission: Spaceborne lidar for  
499 observation of aerosols and clouds, *Proc. SPIE*, **4893**, 1–11.
- 500 Woodward J. L. (2010). *Estimating the Flammable Mass of a Vapour Cloud: A CCPS Concept Book*, John  
501 Wiley & Sons, ISBN 0470935359, 9780470935354.
- 502 Wooster, M. J., G.L.W. Perry and A. Zoumas. (2012) Fire, drought and El Niño relationships on Borneo  
503 (Southeast Asia) in the pre-MODIS era (1980–2000), *Biogeosciences*, 9, 317-340, doi:10.5194/bg-9-  
504 317-2012.



505 **Table 1:** Statistical summary of measured (CALIPSO) smoke plume heights in October 2006, at different  
 506 percentiles of extinction height (top/Z=10%, middle-upper/ Z=30%, median/Z=50%, middle-lower/Z=70%,  
 507 and bottom/Z=90%), over the subset of the Maritime Continent **impacted by smoke (FIRE)**, and **not**  
 508 **impacted by smoke (NO-FIRE)**, based on MISR observations (**Figure 1**). “MEAN” is average, “STD” is  
 509 standard deviation, and percentages XX% are the corresponding distribution’s percentiles. Days which are  
 510 statistical outliers (mean >85% or <15% of at least one variable) are listed as 1<sup>st</sup>, 3<sup>rd</sup>, etc.

	bottom [km]	middle-lower [km]	median [km]	middle-upper [km]	top [km]
<b>FIRE 5%</b>	0.18	0.36	0.56	0.89	1.31
<b>FIRE 10%</b>	0.25	0.49	0.76	1.09	1.53
<b>FIRE 15%</b>	0.31	0.59	0.92	1.29	1.67
<b>FIRE 50%</b>	1.38	1.59	1.83	2.22	2.82
<b>FIRE 85%</b>	2.75	2.92	3.13	3.37	3.70
<b>FIRE 90%</b>	3.14	3.30	3.45	3.72	4.07
<b>FIRE 95%</b>	4.18	4.38	4.70	5.56	5.65
<b>FIRE MEAN</b>	1.68	1.92	2.17	2.50	2.98
<b>FIRE STD</b>	1.59	1.55	1.53	1.54	1.55
<b>NO-FIRE 5%</b>	0.16	0.33	0.48	0.60	0.70
<b>NO-FIRE 10%</b>	0.19	0.38	0.55	0.68	0.87
<b>NO-FIRE 15%</b>	0.21	0.42	0.59	0.77	1.12
<b>NO-FIRE 50%</b>	0.31	0.57	0.83	1.25	1.76
<b>NO-FIRE 85%</b>	1.16	1.64	2.01	2.36	2.85
<b>NO-FIRE 90%</b>	1.65	1.98	2.27	2.60	3.05
<b>NO-FIRE 95%</b>	2.22	2.45	2.73	2.99	3.41
<b>NO-FIRE MEAN</b>	0.97	0.98	1.00	1.02	1.08
<b>NO-FIRE STD</b>	0.65	0.93	1.21	1.53	1.98

511



512 **Table 2:** Summary of measured (CALIPSO) smoke plume heights in October 2006, for days that are  
 513 statistical outliers **mean (>85% or <15%) of all data in bold**, mean (>80% or <20%) of all data in regular  
 514 text. The levels are given as a percentile of extinction height over the subset of the Maritime Continent  
 515 **impacted by smoke** (fire-constrained), based on MISR observations (**Figure 1**).

	bottom (90% Extinction) [km]	middle-lower (70% Extinction) [km]	median (50% Extinction) [km]	middle-upper (30% Extinction) [km]	top (10% Extinction) [km]
<b>FIRE 11<sup>th</sup></b>	2.29	2.54	<b>3.26</b>	<b>4.11</b>	<b>4.93</b>
<b>FIRE 15<sup>th</sup></b>	1.85	2.20			
<b>FIRE 22<sup>nd</sup></b>	<b>2.55</b>	<b>2.85</b>	2.95		

516



517 **Table 3:** Monthly statistics of measured fire properties (FRP and  $T_F$ ), for all measured fires (**ALL**) and  
 518 level 9 confidence fires (**L9**) and MERRA meteorological properties ( $T_A$ ,  $v$ ,  $U$ ,  $dT/dz$ ) corresponding to the  
 519 geographic locations of **L9**. All data is constrained by the boundaries of the fire extent in October 2006  
 520 (**Figure 1**). The distribution's percentile is given as "**XX%**", the mean and standard deviation are given as  
 521 "**MEAN**" and "**STD**". Note that there were no observed fires of **L9** on the following dates: 17<sup>th</sup>, 22<sup>nd</sup>, 23<sup>rd</sup>,  
 522 24<sup>th</sup>, 25<sup>th</sup>, 26<sup>th</sup>, 27<sup>th</sup>, 29<sup>th</sup>, 31<sup>st</sup>.

	FRP ALL [W/m <sup>2</sup> ]	FRP L9 [W/m <sup>2</sup> ]	$T_F$ ALL [K]	$T_F$ L9 [K]	$T_A$ L9 [K]	V L9 [mm/s]	U L9 [m/s]	$dT/dz$ L9 [K/km]
<b>5%</b>	95.	140.	370.	410.	296.0	0.2	4.1	-5.25
<b>10%</b>	115.	185.	390.	445.	296.4	0.4	4.4	-5.27
<b>15%</b>	130.	230.	400.	480.	296.6	0.6	4.5	-5.28
<b>50%</b>	300.	540.	535.	725.	298.4	1.5	6.0	-5.43
<b>85%</b>	775.	1240.	910.	1275.	301.1	4.1	7.4	-5.65
<b>90%</b>	975.	1495.	1070.	1525.	301.5	4.6	7.7	-5.69
<b>95%</b>	1290.	1855.	1335.	1850.	302.1	5.6	8.1	-5.75
<b>Mean</b>	510.	920.	702.	1029.	298.7	2.1	6.0	-5.44
<b>StD</b>	720.	1340.	573.	1057.	2.0	1.6	1.3	0.16

523



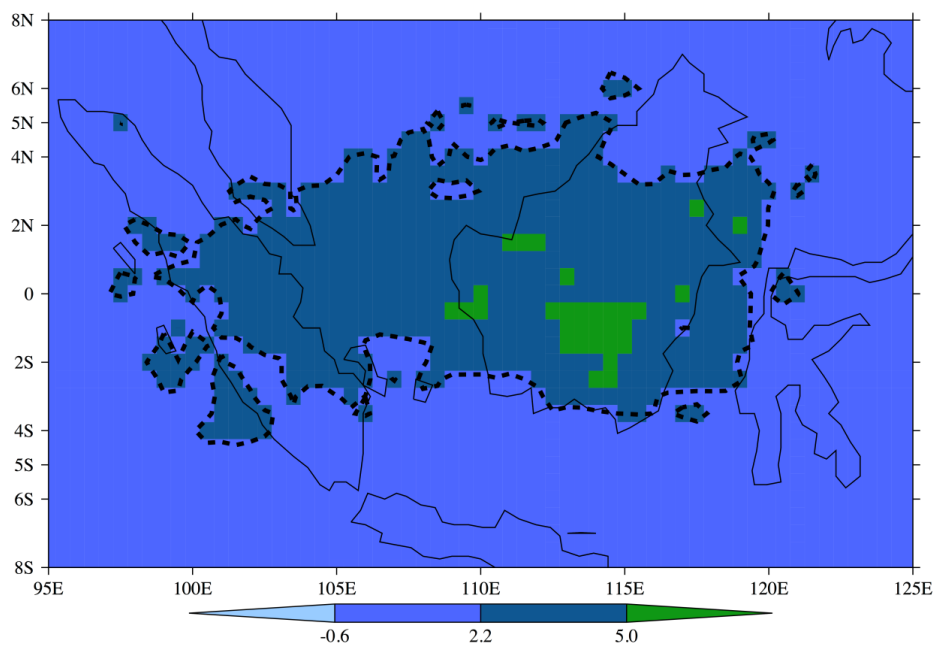
524 **Table 4:** Monthly statistics of modeled aerosol heights, based upon level 9 confidence fires (**L9**) and  
525 MERRA meteorological properties ( $T_A$ ,  $v$ ,  $U$ ,  $dT/dz$ ) at the corresponding geographic locations. Sensitivity  
526 tests are shown with their respective weighting factor (**1.2, 1.4, 1.6, 1.8, or 2.0**) applied to the measured  
527 FRP. The modeled heights are given by percentile from the bottom (5%) to the top (95%), while the mean  
528 and standard deviation are given as “**MEAN**” and “**STD**”. Note that the model was not run on the  
529 following days, during which there were no observed **L9** fires: 17<sup>th</sup>, 22<sup>nd</sup>, 23<sup>rd</sup>, 24<sup>th</sup>, 25<sup>th</sup>, 26<sup>th</sup>, 27<sup>th</sup>, 29<sup>th</sup>, and  
530 31<sup>st</sup>.

	<b>FRP(x1.0)</b> [km]	<b>FRP(x1.2)</b> [km]	<b>FRP(x1.4)</b> [km]	<b>FRP(x1.6)</b> [km]	<b>FRP(x1.8)</b> [km]	<b>FRP(x2)[k</b> <b>m]</b>
<b>5%</b>	<b>0.41</b>	0.44	0.48	0.53	0.56	0.60
<b>10%</b>	<b>0.60</b>	0.67	0.73	0.80	0.85	0.91
<b>15%</b>	<b>0.75</b>	0.83	0.91	0.98	1.05	1.12
<b>30%</b>	<b>1.14</b>	1.28	1.40	1.52	1.63	1.74
<b>50%</b>	<b>1.85</b>	2.07	2.27	2.47	2.65	2.82
<b>70%</b>	<b>2.87</b>	3.23	3.54	3.84	4.12	4.38
<b>85%</b>	<b>4.21</b>	4.66	5.11	5.53	5.87	6.22
<b>90%</b>	<b>4.99</b>	5.54	6.08	6.58	6.97	7.41
<b>95%</b>	<b>6.10</b>	6.79	7.43	7.76	8.16	8.61
<b>Mean</b>	<b>2.41</b>	2.69	2.96	3.21	3.44	3.67
<b>StD</b>	<b>1.98</b>	2.21	2.42	2.62	2.81	2.99

531



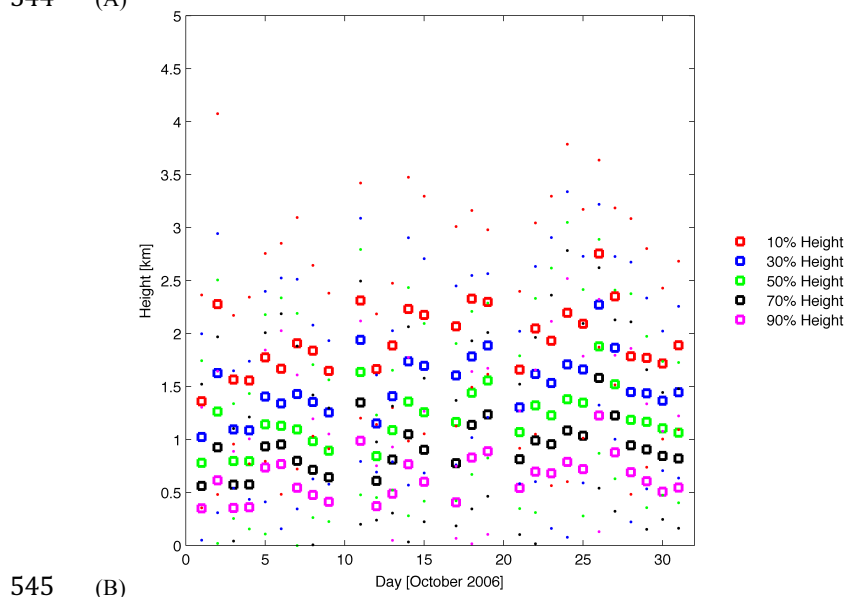
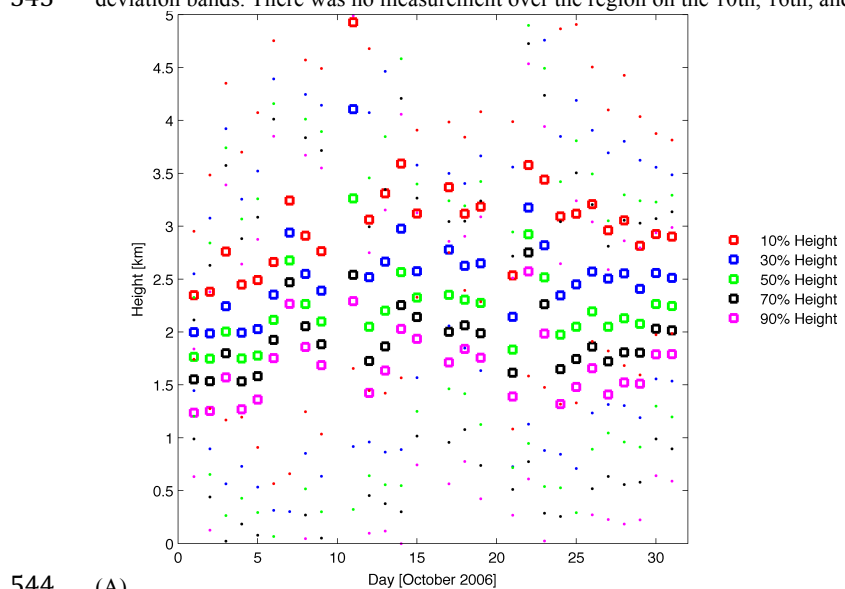
532 **Figure 1:** Map of Maritime Continent. The smoke plume impacts the sub-region contained within the  
533 dashed lines, or the so-called **fire-constrained** region. On the other hand, the region outside of the dashed  
534 lines is the so-called **non fire-constrained** region. The plot is based on a variance maximization technique  
535 applied to the measurements from all MISR overpasses from 2000 through 2014 (*Cohen, 2014*). Note that  
536 in this part of the world 1 degree of latitude or longitude is approximately 100km, leading to a fire-  
537 impacted region over 2500km across.



538



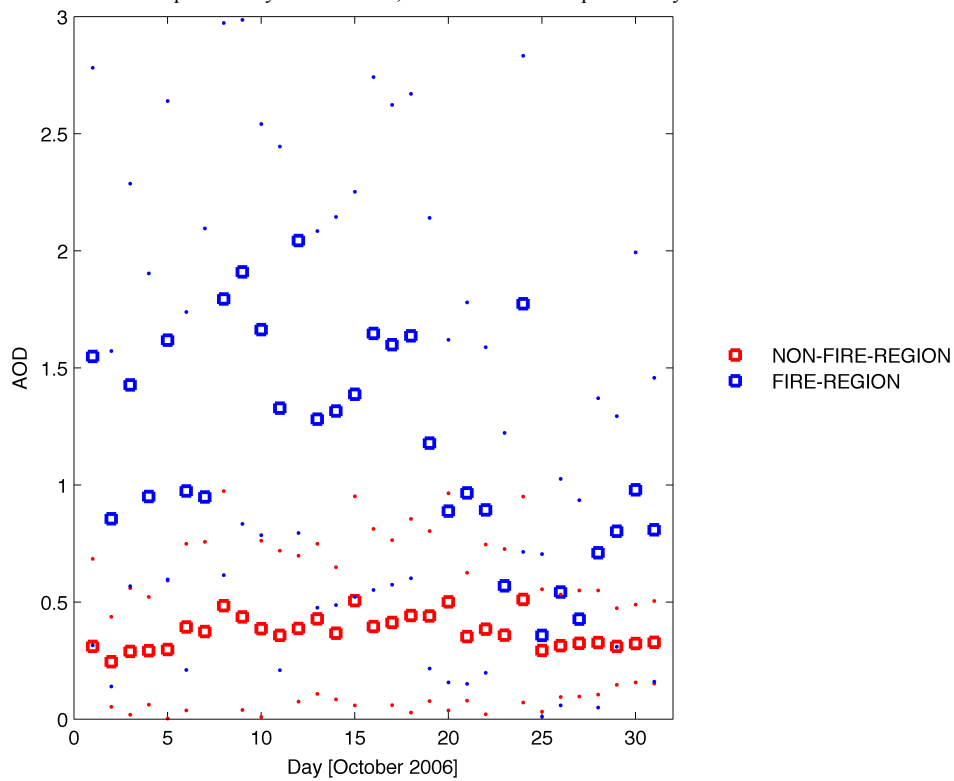
539 **Figure 2a,2b:** Time series of measured CALIPSO extinction heights over the fire constrained (A) and non  
540 fire-constrained (B) regions as given **Figure 1**. For both plots, the dots correspond to the height of the  
541 column integrated backscatter at: 10% [red] (top), 30% [dark blue], 50% [yellow], 70% [black], and 90%  
542 [light blue] (bottom). The circles are computed daily means, while dots are the computed daily standard  
543 deviation bands. There was no measurement over the region on the 10th, 16th, and 20th.







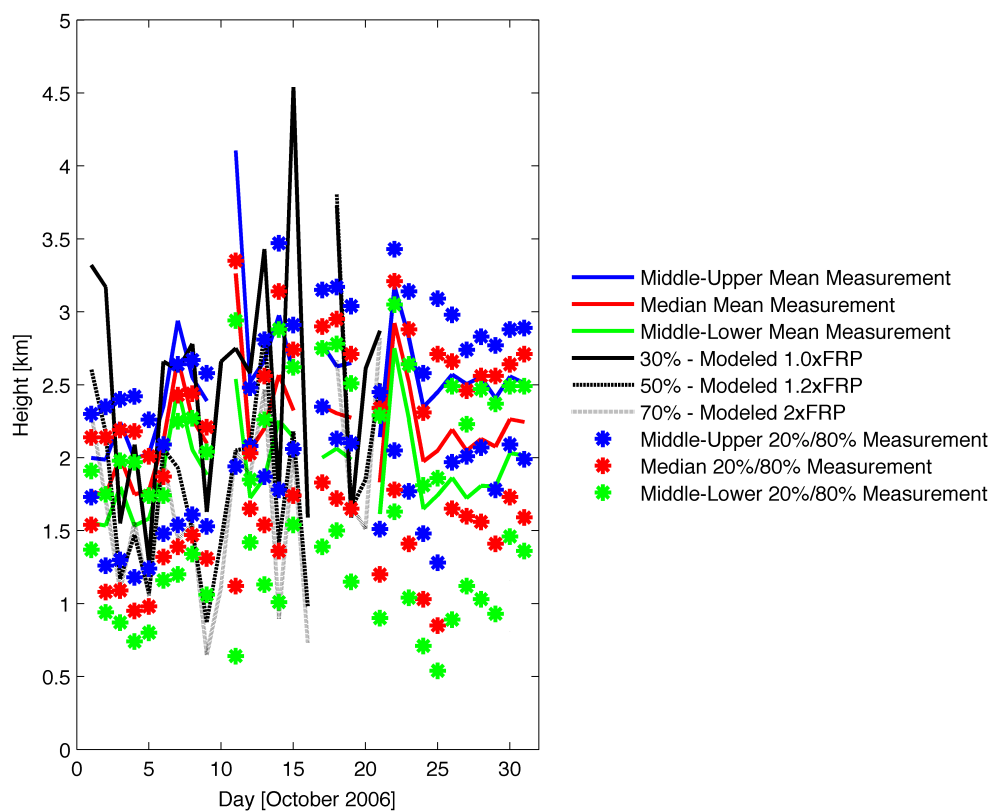
546 **Figure 3:** Time series of daily averaged measured AOD over the fire-constrained regions of the Maritime  
547 Continent [blue], and the non fire-constrained regions of the Maritime Continent [red], as given in **Figure**  
548 **1.** Circles are computed daily mean values, while dots are computed daily standard deviation bands.



549



550 **Figure 4:** Time series of PDFs (20% and 80% values are stars and mean values are given by lines) of the  
551 measured extinction heights for middle-upper (blue), median (red), and middle-lower (green) levels. The  
552 best fitting modeled heights are given as 0% FRP enhancement (solid black line) (best fit for middle-upper  
553 measurements), 20% FRP enhancement (dashed black line) (best fit for median measurements), and 100%  
554 FRP enhancement (dotted black line) (best fit for the middle-lower measurements).



555